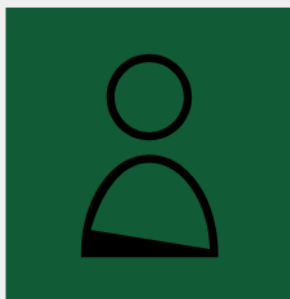


Advancing Characterization of Materials by Multimodal 4D-STEM Analytical Methods

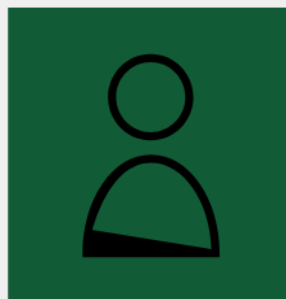
April 26, 11:00am - 12:00pm EDT

Development and production of new materials and semiconductor devices require morphological, structural, and chemical characterization at the nanoscale level to understand their chemico-physical properties and optimize their production process. Besides traditional electron microscopy imaging and compositional analysis techniques, 4D-STEM methods provide additional structural information about the local internal organization of atoms and molecules at each position of an acquired STEM map.

Watch this session during the WAS Virtual Conference:



Dr. Daniel Nemecek



Dr. Tingting Yang

[Register Now](#)

Neutron Reflectivity and Performance of Polyamide Nanofilms for Water Desalination

Fabrizia Foglia, Santanu Karan, Manuela Nania, Zhiwei Jiang, Alexandra E. Porter, Robert Barker, Andrew G. Livingston, and João T. Cabral*

The structure and hydration of polyamide (PA) membranes are investigated with a combination of neutron and X-ray reflectivity, and their performance is benchmarked in reverse osmosis water desalination. PA membranes are synthesized by the interfacial polymerization of *m*-phenylenediamine (MPD) and trimesoyl chloride (TMC), varying systematically reaction time, concentration, and stoichiometry, to yield large-area exceptionally planar films of ≈ 10 nm thickness. Reflectivity is employed to precisely determine membrane thickness and roughness, as well as the (TMC/MPD) concentration profile, and response to hydration in the vapor phase. PA film thickness is found to increase linearly with reaction time, albeit with a nonzero intercept, and the composition cross-sectional profile is found to be uniform, at the conditions investigated. Vapor hydration with H₂O and D₂O from 0 to 100% relative humidity results in considerable swelling (up to 20%), but also yields uniform cross-sectional profiles. The resulting film thickness is found to be predominantly set by the MPD concentration, while TMC regulates water uptake. A favorable correlation is found between higher swelling and water uptake with permeance. The data provide quantitative insight into the film formation mechanisms and correlate reaction conditions, cross-sectional nanostructure, and performance of the PA active layer in RO membranes for desalination.

1. Introduction

Separation processes represent $\approx 45\%$ of energy usage in downstream petrochemical and manufacturing processes,^[1] with membrane-based separations generally offering efficient strategies to decrease energy requirements and environmental footprint.^[1]

Specifically, as less than 1% of the Earth's water is considered to be "fresh",^[2] desalination and waste water treatments are pressing societal challenges, required to meet the growing demand for fresh water for human consumption, agriculture, and industry. These are increasingly met by membrane processes, including reverse osmosis (RO), nanofiltration (NF), and electrodialysis (ED), over traditional thermal and vacuum distillation technologies. Over the past decades, membrane performance for water desalination has improved by a few orders of magnitude, while maintaining economically attractive productivities.^[3] In recent years, RO has emerged as the leading membrane technology for new desalination plants for

both brackish and sea water, as well as in wastewater treatment and organic contaminant removal.^[2–9]

A major challenge faced by RO membrane technologies remains, however, a reduction in energy consumption, associated with the required operation pressure, and a reduction in performance losses during operation, in order to improve process efficiency.^[10–12] Further, variations in water supply (including salinity and foulants), plant location, pretreatment, and waste disposal requirements, demand RO membrane and process optimization tailored for the specific context.^[13–15] Despite considerable research in RO membrane structure and transport,^[10] our fundamental understanding and thus ability to achieve high selectivity (in addition to high permeability) and, in turn, reduce the energy consumption of separation processes and improve performance^[16,17] remains limited and progress has been largely empirical.^[10]

RO membranes comprise a "tight" separating polymeric layer on a more "open" support layer (generally polysulfone), mounted on a woven fabric backing (generally polyester).^[10,18–20] The separating or active layer is usually manufactured by interfacial polymerization (IP) at the organic/aqueous interface

Dr. F. Foglia,^[†] Dr. S. Karan, M. Nania, Z. Jiang, Prof. A. G. Livingston,

Dr. J. T. Cabral

Department of Chemical Engineering

Imperial College London

London SW7 2AZ, UK

E-mail: j.cabral@imperial.ac.uk

Dr. A. E. Porter

Department of Materials

Imperial College London

London SW7 2AZ, UK

Dr. R. Barker^[††]

Institut Laue Langevin

38042 Grenoble, France

^[†]Present address: Institute of Pharmaceutical Science, King's College London, London, UK

^[††]Present address: School of Science and Engineering, University of Dundee, Dundee, UK

 The ORCID identification number(s) for the author(s) of this article can be found under <https://doi.org/10.1002/adfm.201701738>.

DOI: 10.1002/adfm.201701738

between an aromatic diamine (*m*-phenylenediamine, MPD) and trimesoyl chloride (TMC). IP is a polycondensation process between two multifunctional monomers dissolved in immiscible solvents (generally an aqueous and an organic phase) that takes place at the interface between the two solvents. Formally, the organic-soluble component (acid chloride) is insoluble into the polymer, whereas the water-soluble component (diamine) diffuses through the film to react with the acid chloride at the film/organic phase interface, where the film grows.^[21,22] The resulting cross-linked polyamide (PA) film has an overall “apparent” film thickness of, typically, a few hundred nm, and is rough and crumpled, with individual PA film thickness of the order of 10 nm, as revealed by recent high-resolution imaging reports,^[23–26] supported by a porous polysulfone layer with a heterogeneous nanoscale interface layer.^[27]

Despite being widely used on an industrial scale, membranes obtained via IP are generally inhomogeneous in terms of spatial variation, chemistry, and porosity at the micrometer to nanoscales.^[28,29] Although the interplay between the top layer and porous support is important for the membrane properties and, for instance, the support layer undergoes compaction during operation^[10] thus contributing to a reduction in flux, the actual separation process is governed by the PA skin layer. Therefore, a molecular-level understanding of the structure and chemistry^[25,28–31] of this layer is critical to enable the design of novel membranes with superior water desalination performance.^[25,30,31] Toward this goal, considerable effort has been dedicated to the structural characterization of the skin layer of commercially available RO membranes,^[26,28–37] generally carried out under vacuum (away from operating conditions), molecular modeling,^[38–43] or by developing more controlled synthetic pathways.^[37,44–48] These include spin-assisted molecular layer-by-layer (mLbL) techniques,^[37,44,45] and ultrathin films synthesized on Cd(OH)₂ nanowires^[46] and carbon nanotube supports,^[47] or a cellulose nanocrystal interlayer,^[48] seeking to fabricate highly controlled PA thin films, and systematically correlate film thickness, roughness, and membrane performance. By tuning the reaction stoichiometry and time, and thus roughness, a favorable correlation between surface area and membrane flux has been proposed,^[46] suggesting a powerful route to manufacture thin film membranes with high permeance. Crumpled nanofilms polymerized under such controlled interfacial reaction conditions yielded acetonitrile permeances up to 112 L m⁻² h⁻¹ bar⁻¹, two orders of magnitude higher than those of commercially available membranes at equivalent solute retention.^[46]

Since commercial RO membranes typically exhibit a complex, undulated crumpled structure comprising thin films of local thickness of the order of 10 nm, this synthetic route opens possibilities for the direct examination of individual nanofilms within the active layer. With this in mind, our paper seeks to elucidate the nanoscale structure of single PA films, and specifically resolve (i) the cross-sectional composition profile resulting from IP of TMC and MPD and (ii) the membranes response to water, in terms of dimensional changes and the distribution of water throughout the sample, and (iii) evaluate possible correlations with performance.

The planarity and uniformity of the membrane films of ≈10 nm thickness, with footprint in excess of several cm², enables

us, for the first time, to employ neutron and X-ray reflectivity (XRR) to probe the active layer of PA membranes, directly relevant to the RO separation processes. X-ray reflectivity allows a robust quantification of the film thickness and roughness, as well as the scattering length density (SLD) profile with Å resolution.^[35–37,44,45] Combined with neutron reflectivity (NR) and isotopic contrast variation, we are able to resolve the membrane structure and selectively elucidate its various components, under dry and hydrated states, for various reactant stoichiometries and reaction times. Assisted by membrane salt rejection and flux measurements, a mechanistic understanding of the PA active layer structure and its relation to performance emerges.

2. Results and Discussion

2.1. Dry PA

The fabrication of PA nanofilms by nanowire-supported IP is illustrated in **Figure 1a** (detailed in Figure S1, Supporting Information), yielding thickness of the order of 10 nm (Figure 1b), commensurate with film thicknesses of corrugated PA skin layers in RO membranes (Figure 1c). These planar thin films, with sub-nm surface roughness (detailed in Figure S2, Supporting Information), were subsequently floated and transferred onto polished silicon wafers for characterization via reflectometry.

X-ray and neutron reflectivity were employed to elucidate the mechanism of membrane formation, the evolution of film thickness, its possible asymmetry and heterogeneity associated with IP, and response to the ingress of water, with Å resolution. It has been suggested that IP proceeds via cluster formation, aggregation, and percolation,^[40,43,49,50] which have been analytically and numerically modeled. Karode et al.^[51] proposed that TMC/MPD “polymer primary particles” (oligomeric clusters) are initially formed and then coalesce to yield a “coherent film,” via a nucleation process which is concentration dependent.

The initial stage is thought to evolve as a diffusion-limited aggregation (DLA) process, creating dense “colloidal” particles, with active functional groups at the surface, which then aggregate into a lower density structure.^[49,50] The latter yields an inhomogeneous film, exhibiting functional group asymmetry and surface polarization.^[40]

Upon film formation, reactant transport from the aqueous phase across the incipient film barrier becomes severely hindered, limiting further film growth at the organic interface. As a result, the evolution of film thickness with time is highly nonlinear, comprising an initial fast regime, followed by a much slower, asymptotic growth stage. Predictions for the limiting film thickness and the asymmetric distribution of density and charge have been proposed.^[49]

Experimentally, we resolve the dependence of film thickness with reaction time, between 1 and 20 min and TMC/MPD stoichiometry, as shown in Figure 1. We have selected reagent concentrations and stoichiometries that lead to flat PA membranes, yet with films with thicknesses comparable to single skin folds of ubiquitous crumpled PA membranes, extensively employed industrially, and with reasonable performance. From

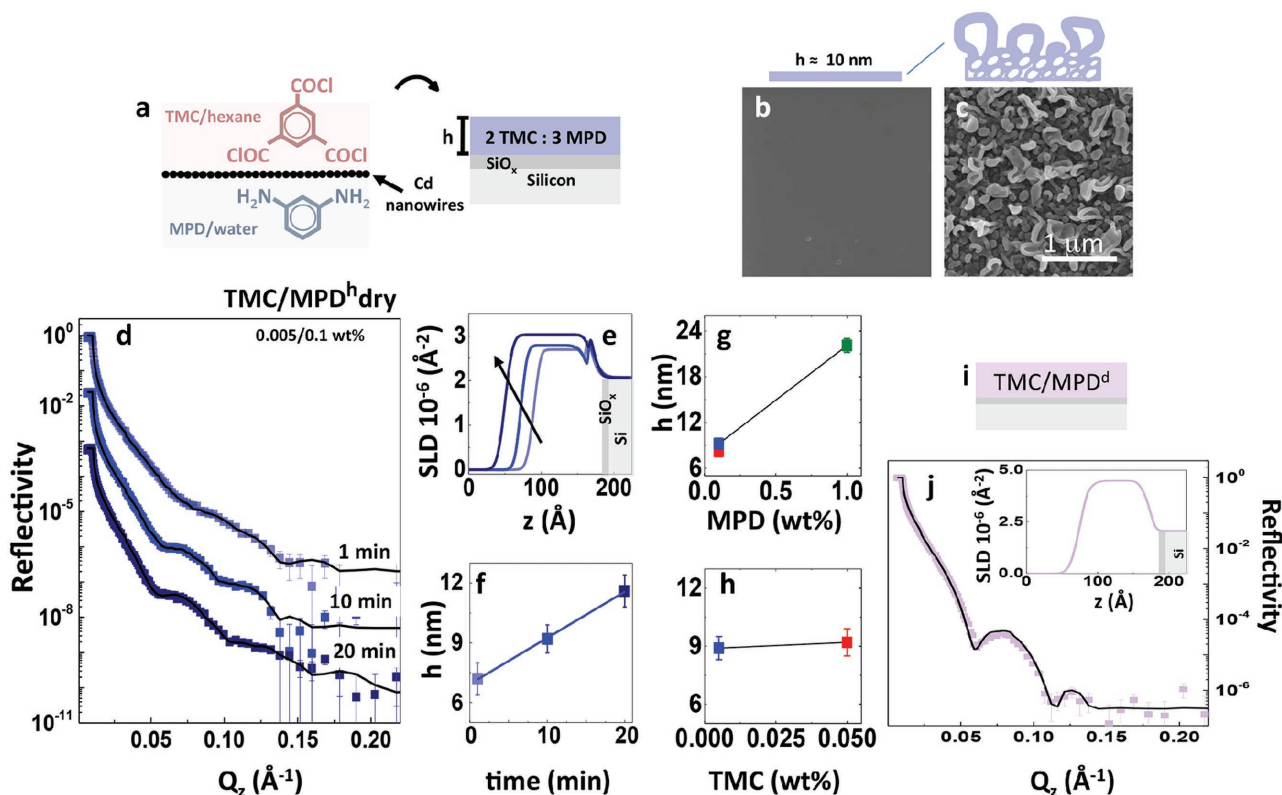


Figure 1. a) Schematic of the interfacial polymerization (IP) reaction between TMC and MPD at the organic/water interface. Smooth, planar PA films with thickness h are transferred onto a Si/SiO_x support for reflectivity. b) SEM picture of smooth nanofilm from TMC/MPD (0.005/0.1 wt%, 10 min reaction time) on polysulfone. c) SEM picture of crumpled nanofilm from TMC/MPD (0.15/3 wt%, 10 min reaction time) on polysulfone. d) NR data and model fits for dry TMC/MPD 0.005/0.1 wt% films obtained at reaction times 1, 10, and 20 min. e) Corresponding SLD profile, where z is the distance normal to the film surface. f) Film thickness h dependence on the reaction time. g) Variation of h with MPD concentration after 10 min reaction time, with TMC 0.005 (blue, green) and 0.05 (red) wt%. h) Variation of h with TMC concentration, with MPD 0.1 wt% (blue, red). i, j) NR of a representative TMC/MPD^d membrane with 0.005/0.1 wt% and reaction time 1 min (corresponding to the first membrane in panel d)), and the SLD profile, shown to be uniform across membrane thickness.

a reference reagent ratio TMC/MPD 0.005/0.1 wt% (shown in blue), we explore permutations by changing one reactant concentration at a time, specifically to 0.005/1 (green) and 0.05/0.1 wt%. The NR profile for TMC/MPD (shown here for 0.005/0.1 wt%), depicted in Figure 1d is well described by a single layer with approximately uniform density across the film cross section, shown in Figure 1e, whose thickness increases linearly within the window of reaction times investigated (detailed in Table S1, Supporting Information). A linear extrapolation to reaction time zero would yield film thickness between 6 and 8 nm for the various stoichiometries. For TMC/MPD 0.005/0.1 wt%, shown in Figure 1f, we obtain that the film thickness grows as $h = 0.24t + 6.93$, where h is in [nm], and t is reaction time in [min], within the time window probed. However, at reaction times shorter than 1 min, we do not reliably obtain coherent films with mechanical integrity. These observations corroborate the highly nonlinear nature of the film growth mechanism^[31] and quantify the IP kinetics. We interpret the initial stage to correspond to the cluster formation, reaching a coherent film at ≈ 1 min reaction time, when measurements are first possible, at these low reactant concentrations. We resolve a considerable time window of linear growth, indicating that asymptotic self-limiting growth,

expected due to restriction of amine diffusion across the film,^[31] occurs at even longer reaction times.

Further, the membrane film densifies within these reaction times, as shown by the increase of the characteristic film SLD, shown in Figure 1e, from which the mass density can also be evaluated (Figure S3, Supporting Information). The SLD values obtained are compatible with a fully cross-linked structure with a ratio TMC/MPD 2:3 (Figure S1i, Supporting Information), previously measured by X-ray photoelectron spectroscopy (XPS) on identical membranes.^[46] Upon increasing MPD reactant concentration, the resulting film thickness (at fixed reaction time) increases considerably, as shown in Figure 1g, while the variation in TMC concentration by one order of magnitude has a negligible effect on h , as shown in Figure 1h (detailed in Figures S4 and S5 and in Table S1, Supporting Information).

Hydrogenous TMC/MPD membranes do not enable an evaluation of compositional asymmetry of the membrane along the cross section, due to limited neutron contrast. This can be resolved by selective deuteration of one component, MPD in our case, and NR data and SLD profile are shown in Figure 1i, j. The observed profile indicates a homogenous distribution of MPD and TMC across the film cross section. The simultaneous analysis of the hydrogenous and partially deuterated contrasts

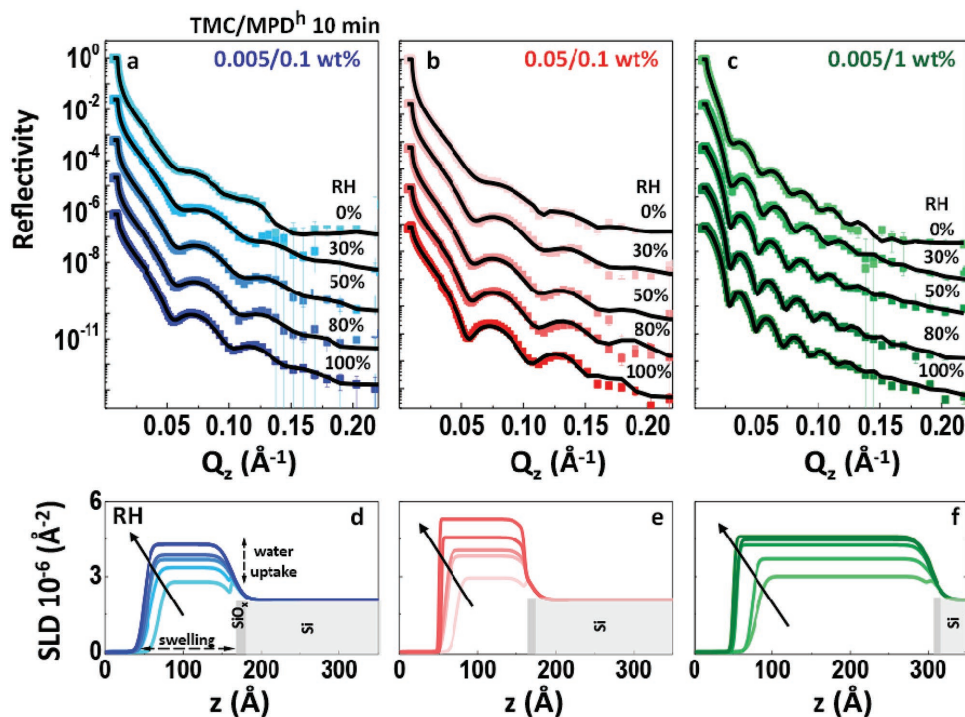


Figure 2. a–c) NR data and model fits for TMC/MPD 0.005/0.1, 0.05/0.1, and 0.005/1 wt% films obtained at reaction time 10 min, as a function of relative humidity (RH). d–f) Corresponding SLD profiles, where z is the distance normal to the film surface. The arrows indicate the increase in SLD due to the heavy water (D_2O) uptake as a consequence of the increase in RH.

enables an unambiguous resolution of the IP film cross section, showing no selective enrichment of components at either interface. More complex (e.g., multilayer) models did not result in a meaningful improvement of the agreement with the data, in either the fully hydrogenous or the partially deuterated case, and were therefore not explored further. All investigated reaction times and stoichiometries yield planar films with sub-nm surface roughness and homogeneous composition along the film cross section. We note, however, that NR measurements are averaged over the relatively large beam footprint ($2 \times 2 \text{ cm}^2$) and thus local (compositional or density) variations within the plane of the film are not resolved. Further, composition variations at the film's top and bottom interfaces, if any, can be estimated to be smaller than the interfacial roughness of $<1 \text{ nm}$ in all cases (detailed in Figures S2 and S3 and in Table S1, Supporting Information).

Collectively, these data provide unique insight into the cross-sectional structure of the PA active layer with \AA resolution. The nonlinear evolution of film thickness and composition homogeneity across the film thickness ($\approx 10 \text{ nm}$) is compatible with the IP models of clusters formation and self-limiting growth, enabling quantitative comparison with simulation^[40,41] and modeling.^[49,51]

2.2. Hydrated PA

We next consider the hydration of PA membranes, focusing on the thin film swelling and water uptake, as well as the possible change in density and water distribution along the film

cross section. We systematically probe the film structure at increasing hydration in an enclosed humidity chamber from 0 to 100% RH. In order to increase measurement precision, we hydrate with heavy water (D_2O). We compute the water uptake independently from the variation in SLD and thickness of the hydrated film h_{RH} as follows. The SLD of the dry PA film is $SLD_{PA} = (n_{PA} N_A \Sigma b_{PA}) / (h_{RH=0} A)$, where n_{PA} is the number of moles of one PA unit ($C_{18}H_{12}O_3N_3$) in the measured sample volume, with corresponding neutron scattering length b_{PA} ; the scattering volume is formally expressed as $h_{RH=0} A$, the product of film thickness at fixed beam footprint A ; N_A is Avogadro's number. Upon hydration, the SLD of the film becomes

$$SLD_{RH} = \frac{n_{PA} N_A b_{PA}}{h_{RH} A} + \frac{n_{D_2O} N_A b_{D_2O}}{h_{RH} A} \quad (1)$$

where b_{D_2O} and n_{D_2O} are the scattering length and number of moles of D_2O in the measured volume, respectively. The hydrated volume is now $h_{RH} A$. Evidently, n_{PA} remains constant while n_{D_2O} increases upon hydration, and we define water uptake as the molar ratio n_{D_2O} / n_{PA} . From the measured film thickness and initial sample mass, the overall and partial densities can be computed as

$$\rho_{TOT(RH)} = \rho_{PA(RH)} + \rho_{D_2O(RH)} = \frac{n_{PA} M_{W(PA)}}{h_{RH} A} + \frac{n_{D_2O} M_{W(D_2O)}}{h_{RH} A} \quad (2)$$

where $M_{W(PA)}$ and $M_{W(D_2O)}$ are the molar masses of the PA unit and D_2O . The value of A is implicit in these calculations, since n are estimated directly from SLD.

NR data for three stoichiometries, at selected reaction time 10 min, are shown in **Figure 2a–c**. The corresponding SLD profiles, **Figure 2d–f**, quantify the membrane swelling and increase in film SLD with RH, from which the water uptake can be determined (detailed in **Figure S6**, **Tables S1 and S2**, Supporting Information). The constant SLD value along the film cross section, at all RH and stoichiometries, unambiguously indicates that water is homogeneously distributed along the direction normal to the film surface (on average, across the plane of the membrane). This finding is in agreement with the observed TMC/MPD composition homogeneity discussed above.

Upon cycling RH, no hysteresis in the data is observed, indicating a reversible and quasi-equilibrium structural response upon membrane hydration and dehydration (at the timescale of several min). These results are corroborated by complementary XRR studies (**Figure S7**, Supporting Information), which further improve the quantification of both h and roughness, owing to the large SLD contrast.

The dry SLD values for films prepared at all reagent stoichiometries are approximately identical, which indicate that the TMC/MPD 2:3 film ratio applies to all conditions. However, the SLD values in each case evolve differently upon hydration which, qualitatively, indicates that the PA film density and/or water uptake with RH depends on reagent stoichiometry. Careful modeling of the NR data enables the quantification of the changes in hydrated film thickness h_{RH} as well as overall and partial densities, and thus decoupling water uptake from film swelling.

These measurements seek to shed light on the packing and free volume^[52] of PA RO membranes and thus finding correlations with solute transport.

Irregular packing and local structural and compositional heterogeneity is predicted to occur during the membrane formation, and thus create density modulations and porosity.^[52] Such voids can be expected to be varying in circularity, openness, and connectivity, and change with treatments such as conditioning, annealing, swelling, and/or pressurization.^[52] Indeed, a discrepancy between the degree of membrane swelling and volume fraction of water uptake has been reported.^[50–52]

Previous molecular dynamics (MD) and Monte Carlo (MC) simulations,^[41,50] and positron annihilation lifetime spectroscopy (PALS) studies^[53] suggest that fully cross-linked PA film exhibits a distribution of cavity sizes, with dimensions of the order of 5 Å, which remains broadly unchanged along the direction normal (z) to the membrane surface, becoming slightly larger at both interfaces. Kim et al.^[53] detected a bimodal pore distribution, of “network” and “aggregate” pores, the former being smaller and related to the geometry of the cross-linked network and the latter being larger and related to film formation. For instance, the addition of dimethyl sulfoxide (DMSO) in the aqueous phase during IP has been found to increase the size and number of network pores and thus increase flux.^[53] Along the plane (xy) of the membrane, water is thus expected to be distributed heterogeneously within the polymeric matrix.^[54]

Our reflectivity results, from which the polymer density and water distribution can be computed, reveal that both are homogeneous along the film normal direction (z), with Å resolution. Lateral (xy) heterogeneity at the nanoscale is not directly probed, as the measurements are averaged over a large representative (illuminated) area with a footprint exceeding cm^2 .

Our SLD profiles of both dry and hydrated PA films indicate uniform polymer and water distributions at all conditions, on average, along the z -direction, and no evidence of possibly larger or more numerous pores (and possibly water) at either interface. While the measurements presented so far were carried out under controlled hydration conditions, supplementary experiments were performed under direct immersion in water yielding similar results with 100% RH (**Figure S8**, Supporting Information).

Quantitative analysis of the SLD data reveals that, for all membranes and stoichiometries investigated, the variation in thickness is not proportional to water uptake. Upon increasing RH, film thickness h increases until reaching an asymptote, as shown in **Figure 3a**, well described by $h = h_0(1 - \exp(-k \text{ RH}))$, where k is a fitting parameter. Evidently, while increasing RH also increases water uptake, shown as a molar (and mass) ratio between water and polymer in **Figure 3b**, this behavior is more complex. The correlation between water uptake and film swelling, shown in **Figure 3c**, is strikingly nonlinear (and can be approximately fitted to an exponential).

In general, we find that increasing reaction time increases the thickness of both the dry and hydrated films, in approximately the same manner at all stoichiometries. Film thickness increases by ≈ 2 nm in all cases (**Figure S9**, Supporting Information). At fixed reaction time, increasing the concentration of MPD in the reaction, keeping TMC constant, correlates with reduced water uptake and swelling, as shown from a comparison between green (TMC/MPD 0.005/1%) and blue (0.005/0.1%) curves (**Figure 3d,e**). Under the same conditions, increasing the TMC concentration the variation in swelling is modest, while uptake increases considerably, visible by comparing the red (TMC/MPD 0.05/0.1%) and blue curves (**Figure 3d,e**). Generally, increasing reaction time decreases film water uptake, as well as swelling (measured as h/h_0), which is clearly shown with the blue (TMC/MPD 0.005/0.1 wt%) sets of data from light (1 min) to dark (20 min reaction time). Overall, **Figure 3c** establishes a broad proportionality between swelling and water uptake, which is unsurprising. However, at comparable swelling, the water uptake can vary significantly with reaction stoichiometry, as shown by the comparison with increasing TMC concentration, between blue (TMC/MPD 0.005/0.1 wt%) and red (0.05/0.1 wt%) curves and at 10 min in **Figure 3c**. All results are tabulated in detail in **Table S2** (Supporting Information). Overall, we find that upon increasing RH, the membranes swell asymptotically and that even when film thickness no longer change considerably, water uptake continues, as highlighted by the nonlinearity of **Figure 3c**.

Karode et al.^[51] previously proposed that, at high reactant concentration in the organic phase, cluster polydispersity decreases with increasing reaction time, after passing through a maximum. In our results, a nonmonotonic dependence of water uptake with reaction time is experimentally observed for the high TMC films (red, TMC/MPD 0.05/0.1 wt%) in **Figure 3b**. By comparison with membranes formed at lower TMC (cf. blue 0.005/0.1 wt% at 10 min), the mass densities and swelling are virtually identical, while the water uptake of the former is considerably higher (**Figure 3d,e**). Cluster polydispersity and association within the film have thus likely an impact in membrane response to water. Our data therefore

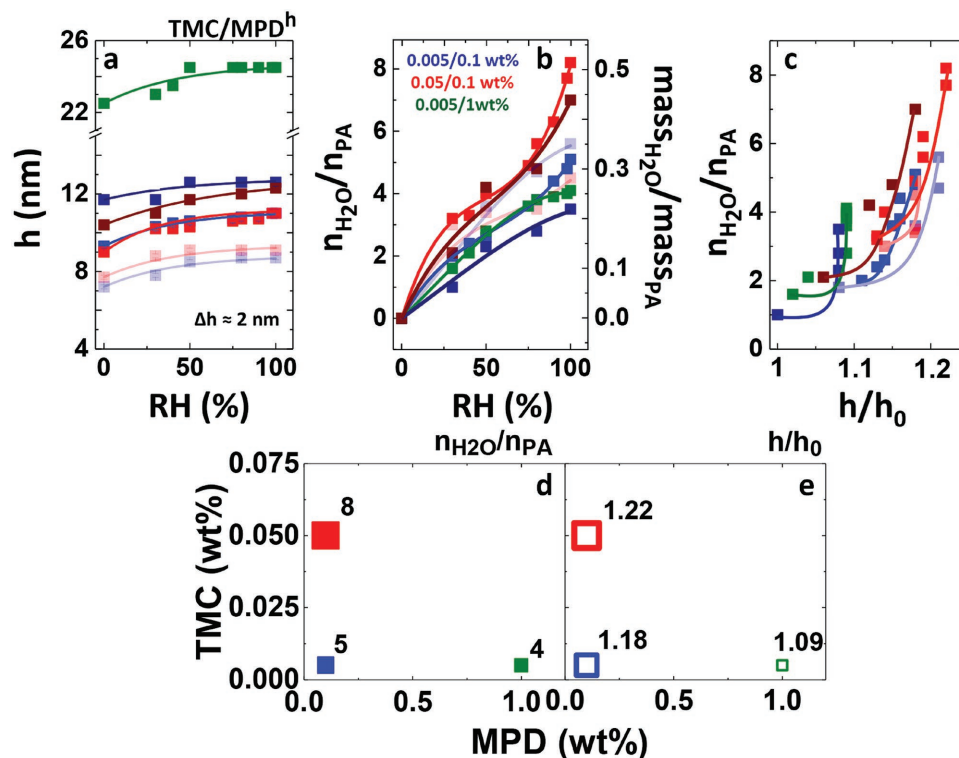


Figure 3. a) Variation of membrane thickness as function of relative humidity; lines are inverse exponential fits. b) Variation of water uptake, shown as both molar and mass ratios, as function of relative humidity (lines are guides to the eye). c) Variation of water uptake as function of membrane swelling. The comparison between the three investigated stoichiometries (TMC/MPD 0.005/0.1, 0.05/0.1, and 0.005/1 wt% thin films; blue, red, and green curves, respectively) is reported for the entire range of reaction times investigated (1, 10, and 20 min; from light to darker colors, respectively); lines are guides to the eye. d) Water uptake and e) membrane swelling as function of the reactant concentration at fixed reaction time (10 min).

suggest that tuning reaction stoichiometry and time, and presumably tuning PA membrane nanostructure, are effective strategies to control film swelling and water uptake (Figure S10, Supporting Information).

To further rationalize the effect of reactant concentration on the film properties, we focus on a fixed reaction time of 10 min in Figure 4 and attempt to correlate data in terms of overall and partial densities. Overall, we have established above that increasing reaction time causes a densification of the membrane (detailed in Table S2, Supporting Information). For clarity, Figure 4a–c replots the dependence of water uptake and swelling at 10 min fixed reaction time, for the three stoichiometries. Significantly, we find that while water uptake follows an approximately linear dependence with RH, membrane swelling does not, saturating at high RH. Combined, we expect these to result in a nonmonotonic change of density with RH, with an initial stage dominated by swelling, which is followed by further water uptake. We therefore compute the partial densities of the polymer ρ_{PA} , water ρ_{H_2O} , as well as the total density ρ_{PA+H_2O} as function of RH, in Figure 4d–f. The polymer partial density, Figure 4d, is computed from the initial polymer mass and film thickness h_0 , upon swelling, that is, from the measured h_{RH} . The total density, Figure 4f, was computed directly from the SLD dependence on RH, at fixed polymer content, enabling the computation of the water partial density, Figure 4e. The lines are self-consistent, simultaneous fits to the data.

Films fabricated with the three stoichiometries evidently exhibit different responses to water. The largest swelling occurs upon initial exposure to water (low RH), while water uptake continues throughout the entire RH range. At the highest MPD concentration (1 wt%), the films exhibit the highest polymer density, as well as the lowest swelling and water uptake (Table S2, Supporting Information). Increasing TMC concentration, at fixed MPD, however, is not found to affect the dry polymer density nor its response to RH (Table S2, Supporting Information). However, the corresponding water uptake changes markedly. While ρ_{H_2O} increases approximately linearly for the blue and green data, corresponding to lower TMC concentration (0.005 wt%), it is clearly nonmonotonic for the red dataset (TMC 0.05 wt%), which has also the highest water uptake. The overall density of the latter reaches a plateau between 30 and 60% RH before increasing further up to 100% RH.

We hypothesize that a higher water uptake might be correlated to a “looser” internal structure in the swollen state, derived from the oligomer formation and cluster organization kinetics into a “coherent” film and the overall nonlinear film thickness evolution. The higher TMC concentration (red dataset) yields films of comparable thickness and density to those of lower TMC (blue dataset) at constant MPD, yet considerable larger water uptake. While the overall film thickness evolution with reaction time is similar in the two cases, the initial reaction kinetics is likely faster at high TMC, which is also compatible with highest h_0 at 1 min (Table S1, Supporting Information).

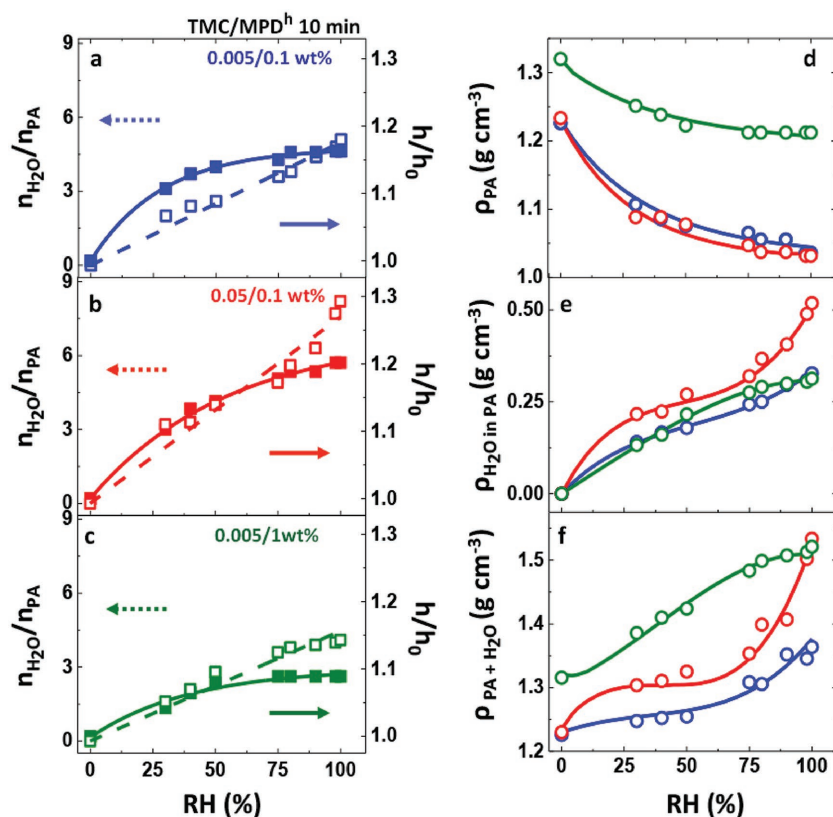


Figure 4. a) Variation of water uptake (molar ratio) and membrane swelling as function of relative humidity for TMC/MPD thin film, at 10 min reaction time, for TMC/MPD 0.005/0.1 wt%, b) TMC/MPD 0.05/0.1 wt%, and c) TMC/MPD 0.005/1 wt%. d) Variation of polymer density as function of membrane swelling for the three thin films at 10 min reaction time (TMC/MPD 0.005/0.1, 0.05/0.1, and 0.005/1 wt%; blue, red, and green curves, respectively). e) Variation of water density within the membrane as function of membrane swelling for the three thin film at 10 min reaction time (TMC/MPD 0.005/0.1, 0.05/0.1, and 0.005/1 wt%; blue, red, and green curves, respectively). f) Variation of total membrane (polymer and water) density as function of membrane swelling for the three thin films at 10 min reaction time (TMC/MPD 0.005/0.1, 0.05/0.1, and 0.005/1 wt%; blue, red, and green curves, respectively).

Faster initial kinetics could thus yield a more “open” structure; however, the two densities are effectively identical, which implies that pore structure and connectivity are likely responsible for the difference. By contrast, increasing MPD (green dataset) yields not only much thicker films, at comparable reaction times, but also denser and therefore with lower swelling and water uptake.

We next seek to correlate the detailed structural analysis reported so far, and its response to hydration, with RO membrane performance, in terms of permeance and salt rejection (Figure 5). Representative thin film membranes, at 10 min reaction time, were evaluated under cross-flow filtration at 20 bar and 2 g L^{-1} NaCl conditions for 100 h. All performance and structural parameters are given in Table S3 and Figure S11 (Supporting Information). We find that the highest permeance is obtained for the membrane films which swell and uptakes most water and have the lowest density (red dataset, with highest TMC wt%). On the other hand, membranes with similar TMC concentration, but different MPD (blue and green datasets), albeit with very different membrane thickness, exhibit similar

permeance (and water uptake), as shown in Figure 5a. By contrast, the highest salt rejection is obtained at low TMC and lower MPD concentrations, as shown in Figure 5b. Based on the findings reported in Figure 4, we find a clear dependence between permeance (or flux) and the water density within the membrane $\rho_{\text{H}_2\text{O}}$ at full hydration, as shown in Figure 5c. Salt rejection, on the other hand, is found to correlate favorably with the inverse of the total hydrated membrane density.

Employing AFM and FT-IR, Dražević et al.^[54] investigated correlations between the swelling of commercial fully and partially aromatic polyamide membranes, as well as poly vinyl alcohol and cellulose acetate films, with water permeability. Despite scatter in the data, a positive correlation between permeability and swelling is found, as well as decrease in salt rejection, rationalized in terms of polymer rigidity and cross-linking. A similar trend has been proposed by Freger et al.^[34] based on polyamide nanofiltration membranes subjected to an acid treatment and reported an increase in flux (and decrease of glucose rejection) with membrane swelling. In this case, a decrease in cross-linking was induced by the acid treatment. Separately, Khorshidi et al.^[25] established that reducing the temperature of the organic phase yields thinner and smoother PA films with a greater degree of cross-linking and higher water flux. However, the reactant concentration employed (TMC/MPD 0.2/2 wt%) differs considerably from the much lower range 0.005–0.05/0.1–1 wt% employed in this work, preventing a direct comparison, as the network formation is expected to depend significantly on MPD diffusivity in the reaction zone.^[25]

Somewhat surprisingly, no simple correlation is found between permeance and membrane swelling (Figure S11, Supporting Information); we should note, however, that our structural measurements are carried out in the absence of applied pressure and water flux, while the performance data are obtained, evidently, under operating conditions. Moreover, the comparison is made between membranes of distinct reactant stoichiometry and well-defined thin films (with similar degree of cross-linking) in their pristine state. Indeed, when comparing membranes at fixed TMC (blue and green points) or MPD (blue and red points) concentration, a linear correlation between membrane permeance and swelling holds. This observation suggests that the IP mechanism and kinetics are fundamentally affected by reaction stoichiometry during film formation, resulting in different network and aggregate pore structure between those specimens. Salt rejection measurements corroborate this assertion. While the membrane with “looser” internal structure (red points) exhibits the lower salt rejection ($\approx 69\%$), membranes with similar dry density and membrane swelling (blue and red points) exhibit great differences

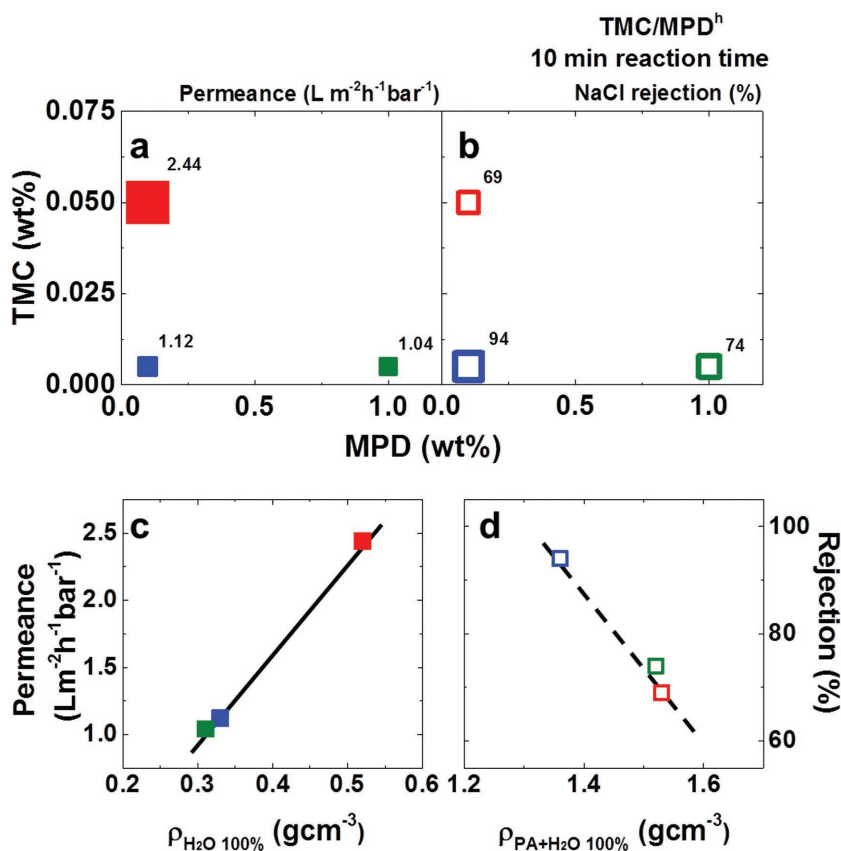


Figure 5. Variation of membrane (a) permeance and (b) NaCl rejection as function of reactant concentration at fixed reaction time (10 min) for the three thin films at 10 min reaction time (TMC/MPD 0.005/0.1, 0.05/0.1, and 0.005/1 wt%; blue, red, and green curves, respectively). c) Variation of membrane permeance as function of water partial density (at 100% RH) for the three thin films at 10 min reaction time (TMC/MPD 0.005/0.1, 0.05/0.1, and 0.005/1 wt%; blue, red, and green points, respectively). d) Variation of NaCl rejection as function of total density (at 199% RH) for the three thin films at 10 min reaction time (TMC/MPD 0.005/0.1, 0.05/0.1, and 0.005/1 wt%; blue, red, and green points, respectively).

in rejection (94 vs 69%); this latter is most likely due to the pore structure and connectivity, likely associated with different kinetics of film formation.

Our data indicate that higher permeance is obtained for stoichiometries exhibiting higher film swelling and water uptake and lower dry mass density. We tentatively interpret these results as due to differences in pore size, shape, and connectivity, which are not directly probed by these experiments, derived from network and aggregate properties that evolve during the nonlinear IP process.

3. Conclusion

Employing a recently developed synthetic route,^[46] we investigate fully aromatic planar PA thin film membranes, obtained under highly controlled IP conditions, with uniform thickness, of the order of 10 nm, and sub-nm roughness, over large surface areas (in excess of cm²). These films can thus be investigated by neutron and X-ray reflectivity, providing unprecedented insight into the membrane structure at sub-nm spatial resolution along

the direction normal to the surface (z), and statistically averaged across the plane of the film (xy) in a representative manner. This structural resolution also permits direct comparisons with theory and computer simulations of IP, allowing quantitative insight into the network formation mechanism and response to water, at the molecular level. We establish for the first time that PA thin films are compositionally homogeneous, on average, along the direction normal to the film surface in both dry and hydrated states. Possible compositional heterogeneity (related to surface polarisation effects) at either interface must thus be limited to <1 nm in depth, that is, commensurate with the interfacial width below which the ability to discriminate between composition and surface roughness is lost.

The evolution of film thickness with reaction time, at all stoichiometries investigated, can be described by a linear dependence within the 1–20 min range, but exhibit a markedly nonzero intercept. Since shorter reaction times do not result in robust membrane films (at these concentrations), we expect this stage to correspond to oligomerization, cluster formation, and aggregation, beyond which “coherent” film are formed and grow. Our longest reaction times evidently do not reach the expected growth asymptote, and the measurement provides quantification of the initial to intermediate growth kinetics. Overall, our results clearly corroborate the mathematical approaches so far presented to model the reaction mechanism.

Different TMC/MPD stoichiometries, however, result in different growth kinetics as well as a range of physical properties, including film swelling and water uptake. We find that while water uptake is broadly proportional to film swelling, this relationship is highly nonlinear, and can be generally described by an exponential dependence. Increasing TMC concentration in the reaction is found to correlate with higher membrane swelling as well as higher water uptake. Increasing MPD concentration, on the other hand, broadly correlates with increasing film thickness and density, within the range investigated. As expected, increasing density decreases the swelling ability in water. The different reaction stoichiometries evidently impact the network formation mechanism and kinetics and thus RO performance, and full 3D structural resolution at sub-nm scale would be required to establish pore network geometry and connectivity, beyond the current 1D measurements. Our data provide unique insight into the relation between reaction conditions (stoichiometry and time), structure, and performance relation of the PA active layer of RO membranes contributing toward the development of quantitative IP models and improved membrane separations.

4. Experimental Section

Membrane Fabrication: Fully aromatic PA films were fabricated by interfacial polymerization of MPD and TMC at a water–hexane interface onto a sacrificial Cd(OH)₂ nanostrand layer supported by an ultrafiltration membrane, following a procedure reported previously.^[46,55] TMC 98% and MPD flakes 99+% were purchased from Sigma-Aldrich (Gillingham, UK). Polyimide polymer (P84) was purchased from HP Polymer GmbH (Austria), and cadmium chloride hydrate, Puratronic, (99.998%) from Alfa Aesar, UK. Spectroscopic grade solvents (VWR International) and deionized water (Millipore) at 18 MΩ cm residual specific resistance were employed.

Interfacial polymerization onto a Cd nanostrand support, with various reaction stoichiometries and reaction times as carried out, following a procedure reported earlier.^[55] Solution concentrations are provided in terms of mass fraction of MPD in water, and TMC in hexane. Specifically, the nanostrand/PSf support layer was first soaked in 25 mL aqueous solutions of 0.1 or 1 wt% MPD. Film formation was then initiated by pouring 25 mL of the organic solution TMC in hexane at 0.005 or 0.05 wt%. Reaction times of 1, 10, and 20 min were investigated. To enhance neutron reflection contrast, selected membranes were synthesized with deuterated MPD, d₄-MPD (Toronto Research Chemicals, Canada). The resulting films were finally cleaned with hexane to remove any unreacted TMC. The sacrificial Cd(OH)₂ nanostrand layer was then removed by dissolution in water acidified to pH < 5 with HCl, also resulting in the detachment of the PSf layer. The floated PA membrane films were then transferred to 3 in., 275 μm Si(100) wafers (Si-Mat, Landsberg/Lech, Germany) for analysis. The SiO_x supports were cleaned by successive ultrasonication in acetone, ethanol, and methanol followed by a final UV–O₃ treatment.

Neutron and X-Ray Reflectivity: Specular NR experiments were performed at the D17 reflectometer at the Institut Laue Langevin (Grenoble, France)^[56] at angles 0.5 and 3.0, covering a momentum transfer normal to the surface ($Q_z = (4\pi/\lambda)\sin\theta$) ranging from 0.006 to 0.3 Å⁻¹. A collimating slit geometry was used such that full use could be made of the coherent summing method for processing the data,^[57] maximizing intensity without loss of resolution for the potentially nonflat samples during time-resolved measurements. An aluminium humidity chamber was employed to probe membrane swelling in situ, within 0–100% relative humidity (RH), using heavy water D₂O (>99.7% D, Goss Scientific, UK) to enhance neutron contrast. Experiments were performed at fixed RH and continually cycling RH, as detailed in the Supporting Information. Complementary XRR experiments were carried out with a PANalytical X'Pert PRO MPD diffractometer/reflectometer equipped with a Cu W/Si parabolic mirror (2.2 kW; λ = 1.54 Å), beam attenuator (Ni 0.125 mm), and plate collimator (0.09°), 40 kV generator power and 40 mA, yielding a similar Q_z range of 0.01–0.3 Å⁻¹. Reflectivity profiles were analyzed by the Abeles method using Motofit^[58] and RasCAL,^[59] enabling simultaneous, self-consistent analysis of datasets.

Membrane Performance: A cross-flow filtration cell with a footprint of 0.001385 m² was operated with a steam of 100 L h⁻¹ containing 2 g L⁻¹ NaCl in water, at a temperature of 30 °C and pressure of 20 bar. Transport data were measured after 100 h, to ensure steady-state conditions.

Supporting Information

Supporting Information is available from the Wiley Online Library or from the author.

Acknowledgements

The authors acknowledge BP International Centre for Advanced Materials (BP-ICAM) for financial support and J. Muscatello, E. Muller, and A. Sutton for useful discussions. We are grateful to the Institut Laue Langevin (Grenoble, France) and ISIS (Oxfordshire, UK) for neutron beamtime.

Conflict of Interest

The authors declare no conflict of interest.

Keywords

neutron reflectivity, polyamide active layers, reverse osmosis

Received: April 2, 2017

Revised: July 4, 2017

Published online: August 2, 2017

- [1] *Materials for Separation Technologies: Energy & Emission Reduction Opportunities*, ORNL, Oak Ridge, TN (USA) **2005**.
- [2] L. F. Greenlee, D. F. Lawler, B. D. Freeman, B. Marrot, P. Moulin, *Water Res.* **2009**, *43*, 2317.
- [3] W. J. Koros, R. P. Lively, *AIChE J.* **2012**, *58*, 2624.
- [4] R. W. Baker, *Membrane Technology and Applications*, 3rd ed., Wiley, Chichester, UK **2012**.
- [5] A. K. Pabby, S. S. H. Rizvi, A. M. S. Requena, *Handbook of Membrane Separations: Chemical, Pharmaceutical, Food and Biotechnological Applications*, 2nd ed., CRC Press, Boca Raton, FL (USA) **2015**.
- [6] W. J. Lau, A. F. Ismail, N. Misdan, M. A. Kassim, *Desalination* **2012**, *287*, 190.
- [7] C. Fritzmann, J. Löwenberg, T. Wintgens, T. Malin, *Desalination* **2007**, *216*, 1.
- [8] S. S. Shenvi, A. M. Isloor, A. F. Ismail, *Desalination* **2015**, *368*, 10.
- [9] M. M. Khin, A. S. Nair, V. J. Babu, R. Murugan, S. Ramakrishna, *Energy Environ. Sci.* **2012**, *5*, 8075.
- [10] R. J. Petersen, *J. Membr. Sci.* **1993**, *83*, 81.
- [11] M. T. M. Pendergast, E. M. V. Hoek, *Energy Environ. Sci.* **2011**, *4*, 1946.
- [12] D. Li, H. Wang, *J. Mater. Chem.* **2010**, *20*, 4551.
- [13] S.-J. Kim, B. S. Oh, H.-W. Yu, L. H. Kim, C.-M. Kim, E.-T. Yang, M. S. Shin, A. Jang, M. H. Hwang, I. S. Kim, *Desalination* **2015**, *370*, 44.
- [14] C. Sun, L. Xie, X. Li, L. Sun, H. Dai, *Desalination* **2015**, *371*, 18.
- [15] D. Cohen-Tanugi, R. K. McGovern, S. H. Dave, J. H. Lienhard, J. C. Grossman, *Energy Environ. Sci.* **2014**, *7*, 1134.
- [16] J. R. Weber, C. O. Osuji, M. Elimelech, *Nat. Rev. Mater.* **2016**, *1*, 1.
- [17] H. B. Park, J. Kamcev, L. M. Roberson, M. Elimelech, B. D. Freeman, *Science* **2017**, *356*, 1137.
- [18] M. Mulder, *Basic Principles of Membrane Technology*, 2nd ed., Springer, Netherlands **1997**.
- [19] I. Pinnau, B. D. Freeman, *Membrane Formation and Modification*, ACS Symposium Series, vol. 744, American Chemical Society, Washington, DC **1999**.
- [20] P. W. Morgan, *Condensation Polymers: By Interfacial and Solution Methods*, John Wiley, New York **1965**.
- [21] P. W. Morgan, S. L. Kwolek, *J. Polym. Sci., Part A: Polym. Chem.* **1996**, *34*, 531.
- [22] J. E. Cadotte, R. S. King, R. J. Majerle, R. J. Petersen, *J. Macromol. Sci., Part A: Pure Appl. Chem.* **1981**, *A15*, 727.
- [23] F. Pacheco, R. Sougrat, M. Reinhard, J. O. Leckie, I. Pinnau, *J. Membr. Sci.* **2016**, *501*, 33.
- [24] A. K. Ghosh, B. H. Jeong, H. Huang, E. M. V. Hoek, *J. Membr. Sci.* **2008**, *311*, 34.
- [25] B. Khorshidi, T. Thundat, B. A. Fleck, M. Sadrzadeh, *Sci. Rep.* **2016**, *6*, 22069.

- [26] M. M. Klosowski, C. M. McGilvery, Y. Li, P. Abellan, Q. Ramasse, J. T. Cabral, A. G. Livingston, A. E. Porter, *J. Membr. Sci.* **2016**, 520, 465.
- [27] X. Lu, S. Nejati, Y. Choo, C. O. Osuji, J. Ma, M. Elimelech, *Appl. Mater. Interfaces* **2015**, 7, 16917.
- [28] V. Freger, *Langmuir* **2003**, 19, 4791.
- [29] O. Coronell, B. J. Mariñas, D. G. Cahill, *Environ. Sci. Technol.* **2011**, 45, 4513.
- [30] S.-Y. Kwak, S. C. Jung, S. H. Kim, *Environ. Sci. Technol.* **2001**, 35, 4334.
- [31] D. G. Cahill, V. Freger, S.-Y. Kwak, *MRS Bull.* **2008**, 33, 27.
- [32] B. Mi, O. Coronell, B. J. Mariñas, F. Watanabe, D. G. Cahill, I. Petrov, *J. Membr. Sci.* **2006**, 282, 71.
- [33] Q. Li, X. Pan, C. Hou, Y. Jin, H. Dai, H. Wang, X. Zhao, X. Liu, *Desalination* **2012**, 292, 9.
- [34] V. Freger, A. Bottino, G. Capannelli, M. Perry, V. Gitis, S. Belfer, *J. Membr. Sci.* **2005**, 256, 134.
- [35] E. P. Chan, A. P. Young, J.-H. Lee, J. Y. Chung, C. M. Stafford, *J. Polym. Sci., Part B: Polym. Phys.* **2013**, 51, 385.
- [36] E. P. Chan, A. P. Young, J.-H. Lee, C. M. Stafford, *J. Polym. Sci., Part B: Polym. Phys.* **2013**, 51, 1647.
- [37] E. P. Chan, S. C. Lee, *J. Polym. Sci., Part B: Polym. Phys.* **2017**, 55, 412.
- [38] F. A. Pacheco, I. Pinnau, M. Reinhard, J. O. Leckie, *J. Membr. Sci.* **2010**, 358, 51.
- [39] V. Kolev, V. Freger, *Polymer* **2014**, 55, 1420.
- [40] J. Muscatello, E. A. Muller, A. A. Mostofi, A. P. Sutton, *J. Membr. Sci.* **2017**, 527, 180.
- [41] M. Ding, A. Szymczyk, F. Goujon, A. Soldera, A. Ghoufi, *J. Membr. Sci.* **2014**, 458, 236.
- [42] Y. Xiang, Y. Liu, B. Mi, Y. Leng, *Langmuir* **2013**, 29, 11600.
- [43] E. Harder, D. E. Walters, Y. D. Bodnar, R. S. Faibish, B. Roux, *J. Phys. Chem. B* **2009**, 113, 10177.
- [44] E. P. Chan, J. H. Lee, J. Y. Chung, C. M. Stafford, *Rev. Sci. Instrum.* **2012**, 83, 114102.
- [45] W. Choi, S. Jeon, S. J. Kwon, H. Park, Y.-I. Park, S.-E. Nam, P. S. Lee, J. S. Lee, J. Choi, S. Hong, E. P. Chan, J.-H. Lee, *J. Membr. Sci.* **2017**, 527, 121.
- [46] S. Karan, Z. Jiang, A. G. Livingston, *Science* **2015**, 348, 1347.
- [47] Y. Zhu, W. Xie, S. Gao, F. Zhang, W. Zhang, Z. Liu, J. Jin, *Small* **2016**, 12, 5034.
- [48] J.-J. Wang, H.-C. Yang, M.-B. Wu, X. Zhang, Z.-K. Xu, *J. Mater. Chem. A* **2017**, <https://doi.org/10.1039/C7TA00501F>.
- [49] V. Freger, S. Srebniak, *J. Appl. Polym. Sci.* **2003**, 88, 1162.
- [50] R. Nadler, S. Srebniak, *J. Membr. Sci.* **2008**, 315, 100.
- [51] S. K. Karode, S. S. Kulkarni, A. K. Suresh, R. A. Mashelkar, *Chem. Eng. Sci.* **1998**, 53, 2649.
- [52] K. Košutić, L. Kaštelan-Kunst, B. Kunst, *J. Membr. Sci.* **2000**, 168, 101.
- [53] S. H. Kim, S.-Y. Kwak, T. Suzuki, *Environ. Sci. Technol.* **2005**, 39, 1764.
- [54] E. Dražević, K. Košutić, V. Freger, *Water Res.* **2014**, 49, 444.
- [55] S. Karan, S. Samitsu, X. Peng, K. Kurashima, I. Ichinose, *Science* **2012**, 335, 444.
- [56] R. Cubitt, G. Fragneto, *Appl. Phys. A: Mater. Sci. Process.* **2002**, M74, S329.
- [57] R. Cubitt, T. Saerbeck, R. A. Campbell, R. Barker, P. Gutfreund, *J. Appl. Crystallogr.* **2015**, 48, 2006.
- [58] A. J. Nelson, *J. Appl. Crystallogr.* **2006**, 39, 273.
- [59] RasCal, <http://sourceforge.net/projects/rscl/> (accessed: May 2015).